

Controlled 3D Buckling of Silicon Nanowires for Stretchable Electronics

Feng Xu,[†] Wei Lu,^{*} and Yong Zhu^{†,*}

[†]Department of Mechanical and Aerospace Engineering, North Carolina State University, Raleigh, North Carolina 27695, United States, and ^{*}Department of Electrical Engineering and Computer Science, The University of Michigan, Ann Arbor, Michigan 48109, United States

ABSTRACT Silicon (Si) nanowire (NW) coils were fabricated on elastomeric substrates by a controlled buckling process. Si NWs were first transferred onto prestrained and ultraviolet/ozone (UVO)-treated poly(dimethylsiloxane) (PDMS) substrates and buckled upon release of the prestrain. Two buckling modes (the in-plane wavy mode and the three-dimensional coiled mode) were found; a transition between them was achieved by controlling the UVO treatment of PDMS. Structural characterization revealed that the NW coils were oval-shaped. The oval-shaped NW coils exhibited very large stretchability up to the failure strain of PDMS (~104% in our study). Such a large stretchability relies on the effectiveness of the coil shape in mitigating the maximum local strain, with a mechanics that is similar to the motion of a coil spring. Single NW devices based on coiled NWs were demonstrated with a nearly constant electrical response in a large strain range. In addition to the wavy shape, the coil shape represents an effective architecture in accommodating large tension, compression, bending, and twist, which may find important applications for stretchable electronics and other stretchable technologies.

KEYWORDS: silicon nanowire · buckling · coil · stretchable electronics · local strain

Electronics that can be stretched and/or conformal to curvilinear surfaces (e.g., biological tissues) has recently attracted broad attention.^{1,2} Success of stretchable electronics depends on the availability of electronic materials and structures that can be highly stretched, compressed, bent, and twisted.^{3–7} Two strategies have been employed to achieve stretchable electronics: one is to increase the intrinsic stretchability of the building blocks such as organic molecules, and the other is to create stretchable architectures out of the otherwise straight, fragile blocks.⁸ It is well-known that inorganic semiconductor materials are brittle and typically fracture under a strain of ~1%, which poses a challenge to incorporate them into stretchable devices. Mechanical buckling has been exploited to enhance the stretchability of silicon (Si) nanoribbons by making them into wavy shape.^{9–11} The wavy structures can be reversibly stretched and compressed to large extent without fracture, with a mechanics that is similar to the motion of an accordion bellows. The buckling strategy

has also been used to develop stretchable metal electrodes.^{12,13}

Si nanowires (NWs) are one of the key building blocks for nanoscale electronic, photonic, and electromechanical devices,^{14–16} due to their excellent electrical,^{17–19} optical,²⁰ and mechanical^{21–23} properties. A variety of flexible (bendable) devices using Si NWs have been developed.^{15,16,24} Our recent work found that vapor–liquid–solid synthesized Si NWs have a diameter-dependent fracture strain up to 12%,²³ which is much higher than their bulk value. This finding suggests that Si NWs hold promising potential for stretchable electronics. Ryu *et al.*²⁵ recently found lateral (or in-plane) buckling of Si NWs on elastomeric substrates. With the formation of wavy (*i.e.*, sinusoidal) structures, Si NWs were found to sustain quite large tensile strains (up to ~27%). However, for a sinusoidal structure, the maximum tensile/compressive strains occur at localized positions (*i.e.*, peaks and valleys) of the waves.³ As soon as the local maxima reach the failure strain, the entire structure fails.

An ideal shape to accommodate large tension and compression would lead to uniform strain distribution along the structure. A coil (helical) spring is one such structure.¹¹ In this paper, we report realization and stretchability study of coiled Si NWs on poly(dimethylsiloxane) (PDMS) substrates for the first time. Si NWs were assembled on top of prestrained PDMS substrates and buckled upon release of the prestrain. Both the three-dimensional (3D) coiled shape and the in-plane wavy shape were obtained in a controlled fashion by tuning the surface properties of PDMS. Very large stretchability (~104% in this work) up to the fracture of PDMS was demonstrated for the Si NW coils, which is more than 15 times the

*Address correspondence to yong_zhu@ncsu.edu.

Received for review November 23, 2010 and accepted December 14, 2010.

Published online December 28, 2010.
10.1021/nn103189z

© 2011 American Chemical Society

intrinsic fracture strain of freestanding Si NWs with the same diameter²³ and about 4 times the reported stretchability of the in-plane wavy Si NWs.²⁵ Furthermore, single NW devices based on coiled NWs were demonstrated with a nearly constant electrical response in a large strain range (from -15.3 to 16.5%). It should be noted that coil shape is energetically favorable for one-dimensional structures (*e.g.*, wires). This paper starts with an analysis of the maximum local strains in the coiled and sinusoidal shapes at the same prestrain, followed by fabrication, stretchability, and electrical response of coiled Si NWs.

RESULTS AND DISCUSSION

Consider that a PDMS slab with an initial length of L_0 is stretched to a length of L_1 (with the prestrain defined as $\varepsilon_{\text{pre}} = (L_1 - L_0)/L_0$). A NW is transferred to the PDMS in the strained direction. When the prestrain is released, the NW could buckle into different shapes (wavy or coiled). Wavelength of the wavy shape (or spacing of the coiled shape) varies with the prestrain following a finite-deformation model, $\lambda = \lambda_0/(1 + \varepsilon_{\text{pre}})$, where λ_0 is the critical wavelength at the onset of buckling and is a function of the NW radius and Young's moduli of the NW and substrate.²⁶ Amplitude of the wavy shape (or radius of the coiled shape) can be determined by the simple accordion mechanics in which the contour length is equal to λ_0 .²⁶ Note that the coiled shape could be circle coil or oval coil (*i.e.*, the projection in the axis direction is a circle or an oval). The wavy and coiled shapes of Si NWs are shown schematically in Figure 1a,b, respectively. Details on calculating the amplitudes (or radii) and maximum local strains for three shapes (sinusoidal wave, circle coil, and oval coil) at a given prestrain are provided in the Supporting Information. Figure 1c plots the calculated maximum local strains as functions of the prestrain up to 104% (the fracture strain of PDMS in our work) for the three shapes. For the wavy shape, the maximum local strain increases almost linearly with the prestrain. Taking the fracture strain of 6.5% (for Si NWs with diameter of 28 nm)²³ as an example, the maximum applicable prestrain is about 40%. By contrast, the maximum local strain of the circle-coiled shape gradually increases with the prestrain and approaches $\sim 2.74\%$ when the prestrain increases to 104%. This is due to the fact that the strain distribution is uniform along the length of the circle coil. For the oval-coiled shape, two ratios of the major and minor radii (1.7 and 2.8) are used as examples. It can be seen that, for both ratios, the maximum local strains are larger than that of the circle coil but much smaller than that of the wavy shape. Moreover, smaller ratio yields smaller maximum local strain at the same prestrain, which is consistent with the fact that the circle coil (with the smallest ratio of one) leads to the smallest maximum local strain. Clearly the coiled shape (both circle

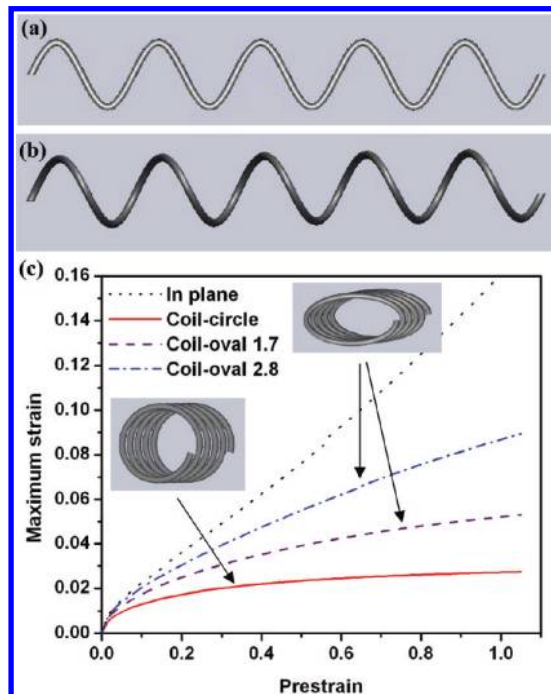


Figure 1. Schematics of (a) wavy and (b) coiled shapes. (c) The maximum local strain of a Si NW as a function of the prestrain up to 104% for in-plane wavy shape, circle-coiled shape, and oval-coiled shape with the ratios of 1.7 and 2.8 between the major and minor radii. The diameter of the NW was set to be 28 nm. The insets show the 3D schematics of the circle coil and oval coil.

and oval) can achieve a much higher level of stretchability than the wavy shape.

To demonstrate the superior stretchability of the coiled shape, coiled Si NWs were fabricated on PDMS substrates. Figure 2a–c shows schematically the process for fabricating buckled NW arrays. A tensile testing stage (Ernest F. Fullam) was used to mechanically stretch the PDMS substrates to the desired levels of prestrain. The prestrained substrate was radiated under a UV lamp (low-pressure mercury lamp, $30 \mu\text{W}/\text{cm}^2$ for 254 nm and $16 \mu\text{W}/\text{cm}^2$ for 185 nm at the distance of 20 cm from the lamp, BHK) with the distance of 7 mm (Figure 2a). A contact printing method was used to dry transfer the Si NWs to the PDMS substrate in the prestrained direction (Figure 2b).²⁷ Releasing the prestrained PDMS resulted in buckling of the Si NWs (Figure 2c). Panels d and e of Figure 2 are optical images showing large-scale Si NWs on the PDMS before and after release of the prestrain, respectively. It can be seen that all the aligned NWs buckled after releasing the PDMS.

Two buckling modes, three-dimensional (3D) coil and two-dimensional (2D) in-plane (sinusoidal) wave, were found in our experiments. Atomic force microscopy (AFM) (in the noncontact mode) and scanning electron microscopy (SEM) were used to interrogate the structure of the buckled NWs, as shown in Figure 3. Figure 3a,b shows the planar and 3D AFM images of a coil-

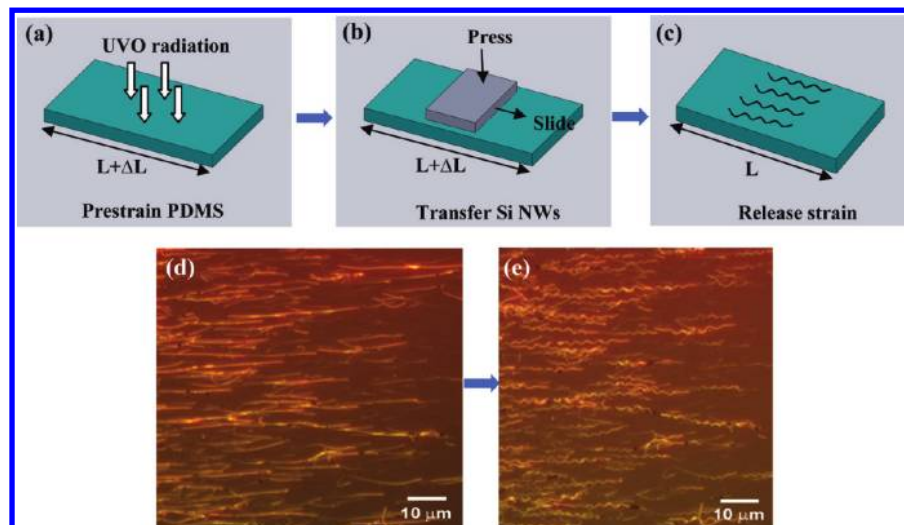


Figure 2. (a–c) Schematic illustration of the process for fabricating the deformed NWs. A large-area optical micrograph of the Si NWs (d) before and (e) after release of the prestrained PDMS substrate.

like NW on PDMS, respectively. The NW showed both in-plane and out-of-plane deformation. Owing to the adaptive nature of the PDMS surface, the NW twisted from one end to the other, resulting in formation of a helical structure. The spacing and width of the coil (except the ends) were quite uniform with an average value of 1523 and 810 nm, respectively. Figure 3c shows two line-scan profiles across the peak and valley of the coil-like NW, as indicated in Figure 3a. The line-scan profiles confirmed that the NW is in a coil configuration. Further, they identified the depth of the coil structure to be 478 nm. By comparing the width and depth of the coil structure, it was concluded that the projected area of the coil in the axial direction is an oval rather than a circle. The ratio between the major radius (width) and minor radius (depth) of the coil was 1.71. Figure 3d shows an SEM image of a typical NW oval coil. Even though part of the NW appears embedded in the PDMS (as marked by an arrow), one can easily imagine how the NW twists to form the coil. A high-magnification SEM image can be found in the Supporting Information. SEM imaging further confirmed that the coil shape of Si NWs is real rather than artifacts from AFM imaging. In contrast, Figure S2a,b (in the Supporting Information) shows planar and 3D AFM images of an in-plane wavy NW, respectively. The corresponding line-scan profile (Figure S2c) and SEM image of a typical wavy NW (Figure S2d) confirmed that the NW is on top of the PDMS without any noticeable out-of-plane deformation. This in-plane buckling mode of Si NWs has been observed previously.²⁵

The buckling modes of Si NWs were found to be controlled by the duration of UV/ozone (UVO) treatment of the prestrained PDMS substrates. Several AFM images in Figure 4 illustrate transition between the two buckling modes at different UVO treatment times (0, 3, 5, 8, and 20 min). The five NWs had similar diameters

(within the range of 30 ± 5 nm) and the PDMS prestrains were all set to be 20%. Without UVO treatment, the NW followed the in-plane wavy mode (Figure 4a). It was noticed that the actual strain as measured from the contour length was $\sim 16\%$ (smaller than the applied prestrain), which is evidence of in-plane sliding of the NW. With increase of the treatment time, NWs gradually exhibited out-of-plane deformation, as can be seen in Figure 4b. At UVO treatment of 5 min, the out-of-plane deformation became pronounced, leading to the oval coiled mode (Figure 4c). However, for further increase of the UVO treatment time, the out-of-plane deformation started to disappear, as shown in Figure 4d. Figure 4e shows a NW at UVO treatment of 20 min, which exhibited the in-plane wavy mode only. Note that, for a given treatment time, all of the NWs with the similar diameters underwent the same transition. Also, the wavelength (or spacing) is approximately constant during the transition except the first case where sliding occurred, as shown in Figure 4.

The total system energy is composed of several parts: the strain energy of the PDMS substrate, the membrane, and bending energies of the Si NW.^{25,26,28} For the coiled mode, additional torsion energy of the Si NW exists. The buckling modes are determined as a result of the minimization of the total system energies. Note that the coil mode is energetically favorable only for one-dimensional structures. The strain energy of PDMS depends on its Young's modulus. UVO treatment leads to the formation of a continuous "silica-like" layer on the surface of PDMS.²⁹ As a consequence, Young's modulus of the PDMS surface was found to increase with the increasing treatment time.³⁰ On the other hand, the sliding as observed in Figure 4a changes the bending and membrane energies of the Si NW. It is well-known that the UVO treatment can change the surface properties of PDMS.^{31,32} The UV light induced ozone

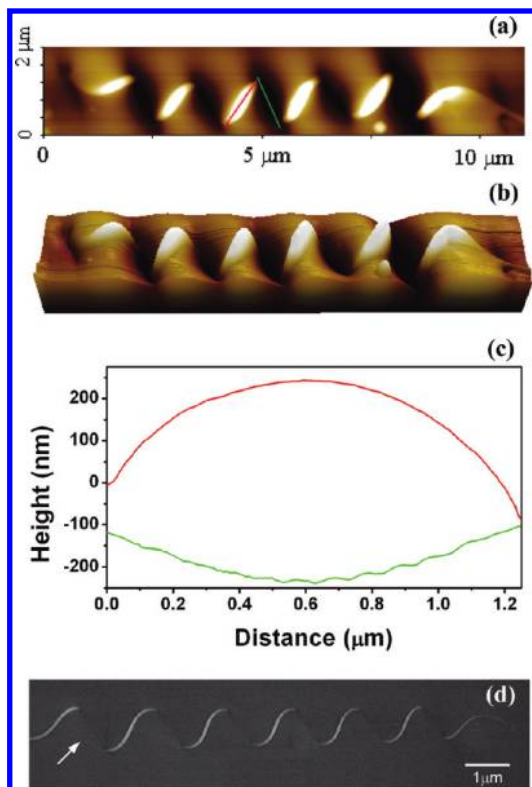


Figure 3. (a) Planar and (b) 3D AFM images of the coil-like Si NWs on PDMS substrate. (c) Line-scan profiles of the AFM image in panel a. (d) SEM image (top view) of a coil-like NW. The arrow marks the part of NW that is embedded in the substrate.

converts the unmodified hydrophobic surface of PDMS dominated by $-\text{Si}(\text{CH}_3)_2\text{O}-$ groups, to a highly polar and reactive surface terminated with silanol groups ($-\text{SiOH}$), which allows reactions with various inorganic surfaces to form strong chemical bonds.³³ In addition, the surface energy of PDMS increases.³² Therefore, the interaction (including static friction) between UVO-treated PDMS and almost all surfaces increases with the treatment time through enhanced chemical bonding and/or van der Waals force.^{9,34} Our recent work found that the shear strength (static friction per unit area) between Si NW and PDMS increased rapidly with increasing UVO treatment time. Details on the study of static friction between Si NW and PDMS will be reported elsewhere.³⁵ Increased static friction between Si NW and PDMS prevented the NW sliding, as shown in Figure 4b–e. In short, the transition between the buckling modes is likely attributed to combined effects of the modified Young's modulus of PDMS surface and static friction between Si NW and PDMS. Further investigation is warranted to understand the relative roles of the Young's modulus and static friction.

Extremely large stretchability was demonstrated for the oval-coiled Si NWs on PDMS. A prestrain just before the failure strain of the PDMS substrate ($\sim 104\%$ in our case) was achieved. Figure 5a shows representative AFM images of a single oval-coiled Si NW stretched

to different levels of tensile strain. The diameter of the NW was estimated to be 28 nm, and the UVO treatment was 5 min. The blue arrows in each AFM image indicate the same positions on the substrate (no sliding between the substrate and the NW) as displacement markers. Figure 5b shows the corresponding plots of the spacing and major and minor radii of the oval-coiled NW as functions of the applied strain. It was found that the spacing increased consistently from 1.52 to 2.68 μm , in linear proportional to the increase of the applied strain. At the same time, the major and minor radii of the oval coil gradually decreased as the applied strain increased, while the ratio between the major and minor radii increased from 1.71 to 2.77. Our results are in good agreement with a nonlinear, finite-deformation model²⁶ in that the wavelength increases in an approximately linear fashion with the prestrain, while the amplitude (major and minor radii in our case) decreases nonlinearly. This model was originally developed to study the buckling mechanics of Si ribbons on PDMS substrate.¹⁰

With the measured parameters including spacing, major, and minor radii of the coil and NW diameter, the maximum local strain of an oval-coiled Si NW at a given applied strain was calculated following the procedure in the Supporting Information and plotted in Figure 5c. It is evident that the maximum local strains are below the failure strain of the Si NW, which indicates that the oval-coil shape is effective in mitigating the maximum strain in the NW and hence explains why coiled Si NWs were capable of achieving such a large stretchability. It is important to point out that the ratio between major and minor radii in the oval-coiled NWs increased (or decreased) with the increasing applied

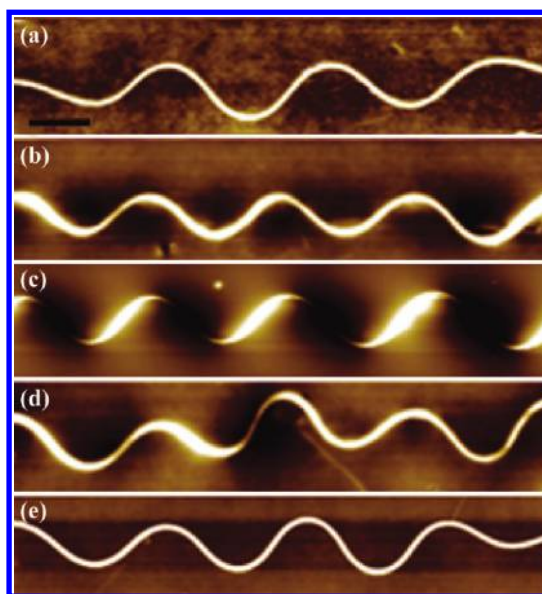


Figure 4. AFM images of deformed Si NWs on the PDMS substrate at different treatment times of (a) 0 min, (b) 3 min, (c) 5 min, (d) 8 min, and (e) 20 min. The prestrains were all set to be 20%. Scale bar is 1 μm .

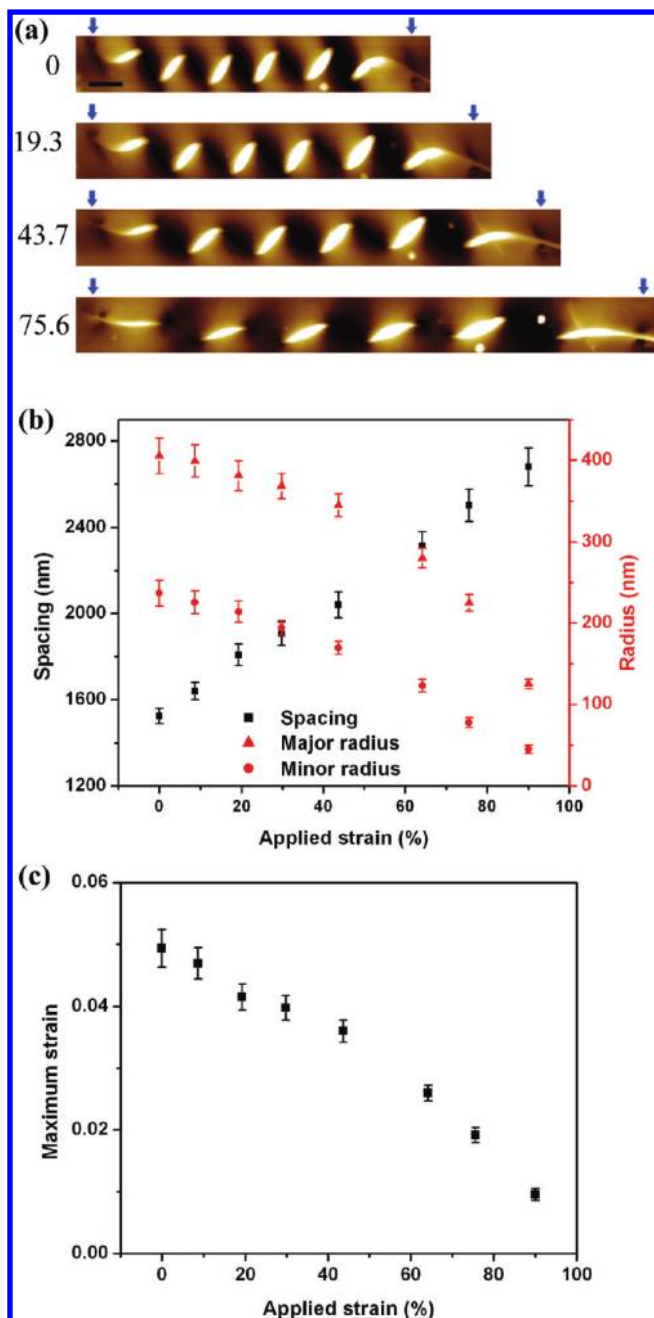


Figure 5. (a) Representative AFM images of an oval-coiled NW stretched to different levels of tensile strain (indicated on the left in percentage). Scale bar is 1 μm . (b) Spacing and major and minor radii of the oval-coiled Si NW as a function of the applied strain. (c) Maximum strain as a function of the applied strain calculated with measured parameters of the oval-coiled NW.

strain (or prestrain). For instance, at the applied strain of 90.1% (or prestrain of 13.9%), the ratio was 2.77, but at the applied strain of zero (or prestrain of 104%), the ratio became 1.71. Note that in our case an applied strain ($\epsilon_{\text{applied}}$) is equivalent to a prestrain with the value equal to $1.04 - \epsilon_{\text{applied}}$. According to Figure 1c, the smaller ratio in an oval-coiled shape is more effective in mitigating the maximum local strain. Therefore, the system seems to be self-adaptive or “smart” to search for an optimized configuration to reduce the maximum

local strain (*i.e.*, at a larger prestrain, the system buckles into an oval coil with a smaller ratio between major and minor radii).

Two-terminal devices were fabricated using coiled Si NWs on a PDMS substrate to demonstrate how these NWs can be integrated into a fabrication process to produce functional, stretchable devices. A layer of Ni (400 nm thick) was evaporated through a shadow mask onto the NW coils to serve as electrodes. In order to improve the electric contact, the devices on PDMS were annealed at 280 $^{\circ}\text{C}$ for 3 min.^{17,36} Figure 6a shows a typical two-terminal device with a single coiled Si NW. Tensile and compressive strains were applied to the PDMS in the NW axial direction by the Fullam mechanical testing stage loaded in a probe station (Micromanipulator). The current–voltage (I – V) response of the Si NW device was measured simultaneously using tungsten probe tips. Figure 6b shows the I – V response as a function of the applied strain (the prestrain in this case was 71.2%). A sequence of images at different strain levels is shown in the Supporting Information. No systematic variation was observed in the electrical properties of the devices when stretched or compressed to a large strain range (from -15.3 to 16.5%, the largest strain range for single NW devices to the best of our knowledge). The scatter of the data is mainly due to variations in the quality of probe contacts. At compressive strains larger than those examined here, the PDMS bent in ways that made probing difficult. At larger tensile strains, the I – V curve changed markedly and did not return to its original state, likely due to change in the contact resistance at the NW–electrode interface and/or formation of cracks in the metal electrodes.^{25,37} However, within the strain range reported above, the device responses did not change appreciably after many cycles of compressing, releasing, and stretching.

Before closing, it should be noted that freestanding helices of semiconductor nanoribbons have been fabricated by scrolling of strained semiconductor heterostructures.³⁸ Other similar nanostructures such as coiled carbon nanotubes and nanowires,^{39,40} SiO₂ nanosprings,⁴¹ and ZnO nanohelices⁴² can be grown by chemical synthesis approaches. However, freestanding coils formed using these methods turned out to be very challenging to be integrated on flat elastomer substrates for stretchable electronics.¹¹

CONCLUSIONS

Here we have demonstrated the feasibility of fabricating oval-coiled Si NWs on PDMS and their resulting excellent stretchability (up to the failure strain of PDMS, $\sim 104\%$ in our study). Clearly according to Figure 1c, the stretchability of the NWs can be further increased if a more stretchable substrate is used. Such a large stretchability of the coiled NWs re-

lies on their effectiveness in mitigating the maximum local strain, with a mechanics that is similar to the motion of a coil spring. The coil shape is instrumental in producing a two-terminal, single NW device that held constant $I-V$ response across a large range of strain (from -15.3 to 16.5%). Future work includes improving the contact reliability at NW-electrode interface and increasing the stretchability of electrodes, such that true functional devices with stretchability over 100% could be possibly achieved. NW-based flexible (bendable) devices have seen rapid progress,^{15,16,24,43,44} now the unique coiled shape makes possible NW-based stretchable devices. Together with the demonstrated NW alignment techniques,^{27,45} coiled NWs offer promising potential for fabricating multilayered devices for stretchable electronics and other related applications. Overall, the coiled shape represents an excellent structural form that can accommodate large tension and compression and likely bending and twist, as well. Although the experiments reported here used Si NWs, this approach should be applicable to other one-dimensional

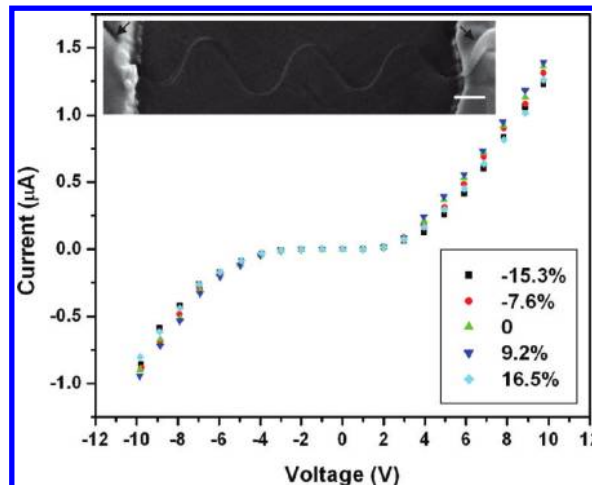


Figure 6. $I-V$ curves of a NW device at different tensile and compressive strains. The inset shows an SEM image of a functional NW device with a single Si NW between two electrodes. The two ends of the NW under the electrodes manifested the out-of-plane deformation (as indicated by arrows). Scale bar is 500 nm.

nanostructures including semiconductor nanowires and carbon nanotubes.

METHODS

Si NW and PDMS Preparation. Boron-doped (p-type) Si NWs were synthesized on Si substrates by chemical vapor deposition (CVD) using gold nanoclusters as catalysts and silane (SiH_4) as a vapor-phase reactant, following the method reported by Wu *et al.*⁴⁶ Poly(dimethylsiloxane) (PDMS) substrates with a thickness of 2 mm were prepared using Sylgard 184 (Dow Corning) by mixing the “base” and the “curing agent” with a ratio of 10:1. The mixture was first placed in a vacuum oven to remove air bubbles and then thermally cured at 65°C for 12 h. Rectangular slabs of suitable sizes were cut from the resultant cured piece.

Acknowledgment. This work was supported by the National Science Foundation under Award Nos. CMMI-0826341 and 1030637. The work at The University of Michigan was supported by National Science Foundation under Award No. ECCS-0804863.

Supporting Information Available: Calculation of the maximum local strains for different shapes at the same prestrain, structural characterization of the coiled NW and in-plane wavy NW, and *in situ* stretching and compression of a coiled NW device. This material is available free of charge *via* the Internet at <http://pubs.acs.org>.

REFERENCES AND NOTES

- Kim, D. H.; Xiao, J. L.; Song, J. Z.; Huang, Y. G.; Rogers, J. A. Stretchable, Curvilinear Electronics Based on Inorganic Materials. *Adv. Mater.* **2010**, *22*, 2108–2124.
- Ko, H. C.; Shin, G.; Wang, S. D.; Stoykovich, M. P.; Lee, J. W.; Kim, D. H.; Ha, J. S.; Huang, Y. G.; Hwang, K. C.; Rogers, J. A. Curvilinear Electronics Formed Using Silicon Membrane Circuits and Elastomeric Transfer Elements. *Small* **2009**, *5*, 2703–2709.
- Gray, D. S.; Tien, J.; Chen, C. S. High Conductivity Elastomeric Electronics. *Adv. Mater.* **2004**, *16*, 393–397.
- Lacour, S. P.; Jones, J.; Wagner, S.; Li, T.; Suo, Z. G. Stretchable Interconnects for Elastic Electronic Surfaces. *Proc. IEEE* **2005**, *93*, 1459–1467.
- Lu, N. S.; Wang, X.; Suo, Z. G.; Vlassak, J. Metal Films on Polymer Substrates Stretched beyond 50%. *Appl. Phys. Lett.* **2007**, *91*, 221909.
- Hu, L. B.; Yuan, W.; Brochu, P.; Gruner, G.; Pei, Q. B. Highly Stretchable, Conductive, And Transparent Nanotube Thin Films. *Appl. Phys. Lett.* **2009**, *94*, 161108.
- Siegel, A. C.; Phillips, S. T.; Dickey, M. D.; Lu, N. S.; Suo, Z. G.; Whitesides, G. M. Foldable Printed Circuit Boards on Paper Substrates. *Adv. Funct. Mater.* **2010**, *20*, 28–35.
- Rogers, J. A.; Someya, T.; Huang, Y. G. Materials and Mechanics for Stretchable Electronics. *Science* **2010**, *327*, 1603–1607.
- Sun, Y. G.; Choi, W. M.; Jiang, H. Q.; Huang, Y. G. Y.; Rogers, J. A. Controlled Buckling of Semiconductor Nanoribbons for Stretchable Electronics. *Nat. Nanotechnol.* **2006**, *1*, 201–207.
- Khang, D. Y.; Jiang, H. Q.; Huang, Y.; Rogers, J. A. A Stretchable Form of Single-Crystal Silicon for High-Performance Electronics on Rubber Substrates. *Science* **2006**, *311*, 208–212.
- Sun, Y. G.; Rogers, J. A. Structural Forms of Single Crystal Semiconductor Nanoribbons for High-Performance Stretchable Electronics. *J. Mater. Chem.* **2007**, *17*, 832–840.
- Bowden, N.; Brittain, S.; Evans, A. G.; Hutchinson, J. W.; Whitesides, G. M. Spontaneous Formation of Ordered Structures in Thin Films of Metals Supported on an Elastomeric Polymer. *Nature* **1998**, *393*, 146–149.
- Lacour, S. P.; Wagner, S.; Huang, Z. Y.; Suo, Z. Stretchable Gold Conductors on Elastomeric Substrates. *Appl. Phys. Lett.* **2003**, *82*, 2404–2406.
- Lu, W.; Lieber, C. M. Semiconductor Nanowires. *J. Phys. D* **2006**, *39*, R387–R406.
- Duan, X. F.; Niu, C. M.; Sahi, V.; Chen, J.; Parce, J. W.; Empedocles, S.; Goldman, J. L. High-Performance Thin-Film Transistors Using Semiconductor Nanowires and Nanoribbons. *Nature* **2003**, *425*, 274–278.
- McAlpine, M. C.; Ahmad, H.; Wang, D. W.; Heath, J. R. Highly Ordered Nanowire Arrays on Plastic Substrates for Ultrasensitive Flexible Chemical Sensors. *Nat. Mater.* **2007**, *6*, 379–384.
- Cui, Y.; Zhong, Z. H.; Wang, D. L.; Wang, W. U.; Lieber, C. M.

- High Performance Silicon Nanowire Field Effect Transistors. *Nano Lett.* **2003**, *3*, 149–152.
18. Zhong, Z. H.; Wang, D. L.; Cui, Y.; Bockrath, M. W.; Lieber, C. M. Nanowire Crossbar Arrays As Address Decoders for Integrated Nanosystems. *Science* **2003**, *302*, 1377–1379.
 19. Wu, Y.; Xiang, J.; Yang, C.; Lu, W.; Lieber, C. M. Single-Crystal Metallic Nanowires and Metal/Semiconductor Nanowire Heterostructures. *Nature* **2004**, *430*, 61–65.
 20. Holmes, J. D.; Johnston, K. P.; Doty, R. C.; Korgel, B. A. Control of Thickness and Orientation of Solution-Grown Silicon Nanowires. *Science* **2000**, *287*, 1471–1473.
 21. Li, X. D.; Bhushan, B. Fatigue Studies of Nanoscale Structures For MEMS/NEMS Applications Using Nanoindentation Techniques. *Surf. Coat. Technol.* **2003**, *163*, 521–526.
 22. Hoffmann, S.; Utke, I.; Moser, B.; Michler, J.; Christiansen, S. H.; Schmidt, V.; Senz, S.; Werner, P.; Gosele, U.; Ballif, C. Measurement of the Bending Strength of Vapor-Liquid-Solid Grown Silicon Nanowires. *Nano Lett.* **2006**, *6*, 622–625.
 23. Zhu, Y.; Xu, F.; Qin, Q. Q.; Fung, W. Y.; Lu, W. Mechanical Properties of Vapor–Liquid–Solid Synthesized Silicon Nanowires. *Nano Lett.* **2009**, *9*, 3934–3939.
 24. McAlpine, M. C.; Friedman, R. S.; Jin, S.; Lin, K. H.; Wang, W. U.; Lieber, C. M. High-Performance Nanowire Electronics and Photonics on Glass and Plastic Substrates. *Nano Lett.* **2003**, *3*, 1531–1535.
 25. Ryu, S. Y.; Xiao, J. L.; Il Park, W.; Son, K. S.; Huang, Y. Y.; Paik, U.; Rogers, J. A. Lateral Buckling Mechanics in Silicon Nanowires on Elastomeric Substrates. *Nano Lett.* **2009**, *9*, 3214–3219.
 26. Jiang, H. Q.; Khang, D. Y.; Song, J. Z.; Sun, Y. G.; Huang, Y. G.; Rogers, J. A. Finite Deformation Mechanics in Buckled Thin Films on Compliant Supports. *Proc. Natl. Acad. Sci. U.S.A.* **2007**, *104*, 15607–15612.
 27. Fan, Z. Y.; Ho, J. C.; Jacobson, Z. A.; Yerushalmi, R.; Alley, R. L.; Razavi, H.; Javey, A. Wafer-Scale Assembly of Highly Ordered Semiconductor Nanowire Arrays by Contact Printing. *Nano Lett.* **2008**, *8*, 20–25.
 28. Huang, Z. Y.; Hong, W.; Suo, Z. Nonlinear Analyses of Wrinkles in a Film Bonded to a Compliant Substrate. *J. Mech. Phys. Solids* **2005**, *53*, 2101–2118.
 29. Graubner, V. M.; Jordan, R.; Nuyken, O.; Schnyder, B.; Lippert, T.; Kotz, R.; Wokaun, A. Photochemical Modification of Cross-Linked Poly(Dimethylsiloxane) by Irradiation at 172 nm. *Macromolecules* **2004**, *37*, 5936–5943.
 30. Song, J.; Tranchida, D.; Vancso, G. J. Contact Mechanics of UV/Ozone-Treated PDMS by AFM and JKR Testing: Mechanical Performance from Nano- To Micrometer Length Scales. *Macromolecules* **2008**, *41*, 6757–6762.
 31. Huck, W. T. S.; Bowden, N.; Onck, P.; Pardoën, T.; Hutchinson, J. W.; Whitesides, G. M. Ordering of Spontaneously Formed Buckles on Planar Surfaces. *Langmuir* **2000**, *16*, 3497–3501.
 32. Efimenko, K.; Wallace, W. E.; Genzer, J. Surface Modification of Sylgard-184 Poly(dimethyl siloxane) Networks by Ultraviolet and Ultraviolet/Ozone Treatment. *J. Colloid Interface Sci.* **2002**, *254*, 306–315.
 33. Ouyang, M.; Yuan, C.; Muisener, R. J.; Boulares, A.; Koberstein, J. T. Conversion of Some Siloxane Polymers to Silicon Oxide by UV/Ozone Photochemical Processes. *Chem. Mater.* **2000**, *12*, 1591–1596.
 34. Xue, C. Y.; Chin, S. Y.; Khan, S. A.; Yang, K. L. UV-Defined Flat PDMS Stamps Suitable for Microcontact Printing. *Langmuir* **2010**, *26*, 3739–3743.
 35. Qin, Q. Q.; Zhu, Y. Static Friction of Silicon Nanowires on Poly (dimethylsiloxane) Substrates. **2010**, submitted.
 36. Zheng, G. F.; Lu, W.; Jin, S.; Lieber, C. M. Synthesis and Fabrication of High-Performance n-Type Silicon Nanowire Transistors. *Adv. Mater.* **2004**, *16*, 1890–1893.
 37. Lee, C. H.; Kim, D. R.; Zheng, X. L. Fabricating Nanowire Devices on Diverse Substrates by Simple Transfer-Printing Methods. *Proc. Natl. Acad. Sci. U.S.A.* **2010**, *107*, 9950–9955.
 38. Zhang, L.; Ruh, E.; Grutzmacher, D.; Dong, L. X.; Bell, D. J.; Nelson, B. J.; Schonenberger, C. Anomalous Coiling of SiGe/Si and SiGe/Si/Cr Helical Nanobelts. *Nano Lett.* **2006**, *6*, 1311–1317.
 39. Gao, R. P.; Wang, Z. L.; Fan, S. S. Kinetically Controlled Growth of Helical and Zigzag Shapes of Carbon Nanotubes. *J. Phys. Chem. B* **2000**, *104*, 1227–1234.
 40. Chen, X. Q.; Zhang, S. L.; Dikin, D. A.; Ding, W. Q.; Ruoff, R. S.; Pan, L. J.; Nakayama, Y. Mechanics of a Carbon Nanocoil. *Nano Lett.* **2003**, *3*, 1299–1304.
 41. Zhang, H. F.; Wang, C. M.; Buck, E. C.; Wang, L. S. Synthesis, Characterization, And Manipulation of Helical SiO₂ Nanosprings. *Nano Lett.* **2003**, *3*, 577–580.
 42. Gao, P. X.; Ding, Y.; Mai, W. J.; Hughes, W. L.; Lao, C. S.; Wang, Z. L. Conversion of Zinc Oxide Nanobelts into Superlattice-Structured Nanohelices. *Science* **2005**, *309*, 1700–1704.
 43. Ju, S. Y.; Facchetti, A.; Xuan, Y.; Liu, J.; Ishikawa, F.; Ye, P. D.; Zhou, C. W.; Marks, T. J.; Janes, D. B. Fabrication of Fully Transparent Nanowire Transistors for Transparent and Flexible Electronics. *Nat. Nanotechnol.* **2007**, *2*, 378–384.
 44. Timko, B. P.; Cohen-Karni, T.; Yu, G. H.; Qing, Q.; Tian, B. Z.; Lieber, C. M. Electrical Recording from Hearts with Flexible Nanowire Device Arrays. *Nano Lett.* **2009**, *9*, 914–918.
 45. Xu, F.; Durham, J. W., III; Wiley, B. J.; Zhu, Y. Strain-Release Assembly of Nanowires on Stretchable Substrates. **2010**, submitted.
 46. Wu, Y.; Cui, Y.; Huynh, L.; Barrelet, C. J.; Bell, D. C.; Lieber, C. M. Controlled Growth and Structures of Molecular-Scale Silicon Nanowires. *Nano Lett.* **2004**, *4*, 433–436.

Controlled 3D Buckling of Silicon Nanowires for Stretchable Electronics

Feng Xu[†], Wei Lu[‡], and Yong Zhu^{†*}

SUPPORTING INFORMATION PARAGRAPH

Calculation of the maximum local strains for different shapes at the same prestrain

1) Sinusoidal shape

The NW shape is described by

$$y = A \cos kx \quad (\text{S3})$$

where the amplitude A and wave number k are to be determined, $k = 2\pi/\lambda$ with λ the wavelength.

If one waveform represents a unit cell, the contour length of the unit cell is equal to the buckling wavelength at the onset of buckling, λ_0 following the geometric compatibility, viz.,

$$\lambda_0 = \int_0^\lambda \sqrt{1 + y'^2} dx = \int_0^\lambda \sqrt{1 + (Ak \sin kx)^2} dx \quad (\text{S4})$$

The prestrain ε_{pre} is written as

$$\varepsilon_{pre} = \frac{\lambda_0 - \lambda}{\lambda} \quad (\text{S5})$$

For a given prestrain ε_{pre} and critical wavelength λ_0 , the wavelength λ is determined by Eq. (S5)

and then the amplitude is determined by Eq. (S4). The curvature along the sine wave is given by

$$K = \frac{y''}{(1 + y'^2)^{3/2}} = -\frac{Ak^2 \cos kx}{[1 + (Ak \sin kx)^2]^{3/2}} \quad (\text{S6})$$

The maximum curvature is

$$K_{\max} = Ak^2 \quad (\text{S7})$$

The maximum strain along the sinusoidal wave is then given by

$$\varepsilon_{\max} = RK_{\max} \quad (\text{S8})$$

2) Circle-coiled shape

An arbitrary point along the circle coil has spatial coordinates of $[R \cos \theta, R \sin \theta, H\theta]$, where R is the in-plane radius, θ is the radial angle ranging from 0 to 2π for one unit cell and $H = h/2\pi$ with h the spacing (wavelength) of the unit cell. The tangential direction at this point is $(-R \sin \theta, R \cos \theta, H)$. The contour length of a unit cell is given by

$$\lambda_0 = \int_0^{2\pi} \sqrt{x(\theta)^2 + y(\theta)^2 + z(\theta)^2} d\theta = 2\pi\sqrt{R^2 + H^2} \quad (\text{S9})$$

For a given prestrain ε_{pre} and critical wavelength λ_0 , the wavelength λ is determined by Eq. (S5) and then the amplitude is determined by Eq. (S9). The curvature along the spiral is constant, given by

$$K = \frac{[(z'' y' - y'' z')^2 + (x'' z' - z'' x')^2 + (y'' x' - x'' y')^2]^{1/2}}{(x'^2 + y'^2 + z'^2)^{3/2}} = \frac{R}{R^2 + H^2} \quad (\text{S10})$$

Therefore, the strain is also constant following Eq. (S8).

3) Oval-coiled shape

An arbitrary point along the oval coil has spatial coordinates of $[a \cos \theta, b \sin \theta, H\theta]$, where a is the major radius, b is the minor radius, θ is the radial angle ranging from 0 to 2π for one unit cell and $H = h/2\pi$ with h the spacing (wavelength) of the unit cell. The tangential direction at this point is $(-a \sin \theta, b \cos \theta, H)$. The contour length of a unit cell is given by

$$\lambda_0 = \int_0^{2\pi} \sqrt{x(\theta)^2 + y(\theta)^2 + z(\theta)^2} d\theta \quad (\text{S11})$$

For a given prestrain ε_{pre} and critical wavelength λ_0 , the wavelength λ is determined by Eq. (S5)

and then the amplitude is determined by Eq. (S11). The curvature along the spiral is given by

$$K = \frac{[(z'' y' - y'' z')^2 + (x'' z' - z'' x')^2 + (y'' x' - x'' y')^2]^{1/2}}{(x'^2 + y'^2 + z'^2)^{3/2}} \quad (S12)$$

$$= \frac{[(bH \sin \theta)^2 + (aH \cos \theta)^2 + (ab)^2]^{1/2}}{[(a \sin \theta)^2 + (b \cos \theta)^2 + H^2]^{3/2}}$$

The maximum and minimum curvatures are given by, respectively,

$$K_{\max} = k|_{\theta=0} = \frac{a}{b^2 + H^2} \quad (S13a)$$

$$K_{\min} = k|_{\theta=\pi/2} = \frac{b}{a^2 + H^2} \quad (S13b)$$

Similarly, the maximum strain can be obtained following Eq. (S8). In all the analyses above, no sliding between the NW and the substrate is assumed.

Structure of the coiled NW

Figure S1 is an SEM image of the coil-like Si NW as shown in Fig. 3(d) at higher magnification. Part of the NW appears embedded in the PDMS. A thin layer of metal coating might contribute to the appearance of embedding (the metal layer is required to eliminate charging).

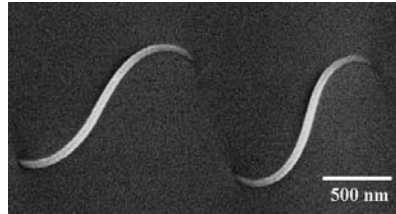


Figure S1 High-magnification SEM image of the coil-like Si NW as shown in Fig. 3(d).

Structure of the in-plane wavy NW

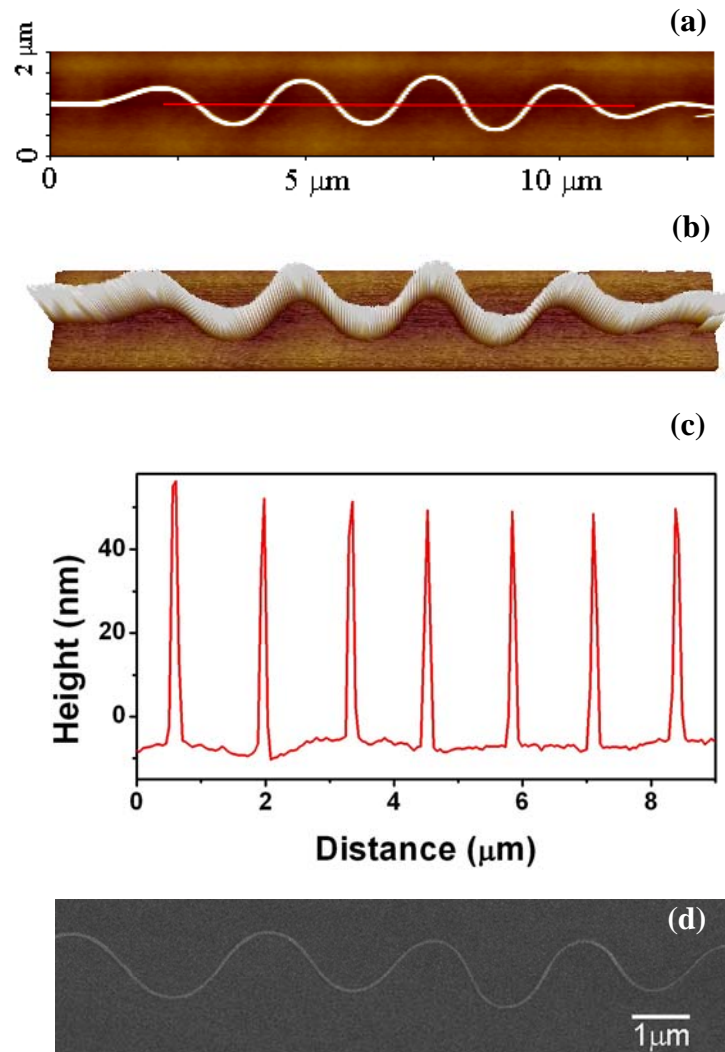


Figure S2 (a) Planar and (b) 3D AFM images of the wavy Si NW on PDMS substrate. (c) Line-scan profile of the AFM image in a. (d) SEM image of the wavy NW.

Stretch and compression of a coiled NW device

A sequence of optical images the coiled NW device at different strain levels are shown in Figure S3, corresponding to the I-V curve in Figure 6. It can be clearly seen that the NW was stretched or compressed. The last image shows that the NW was stretched to the level of the prestrain (i.e., the nanowire was stretched to be straight).

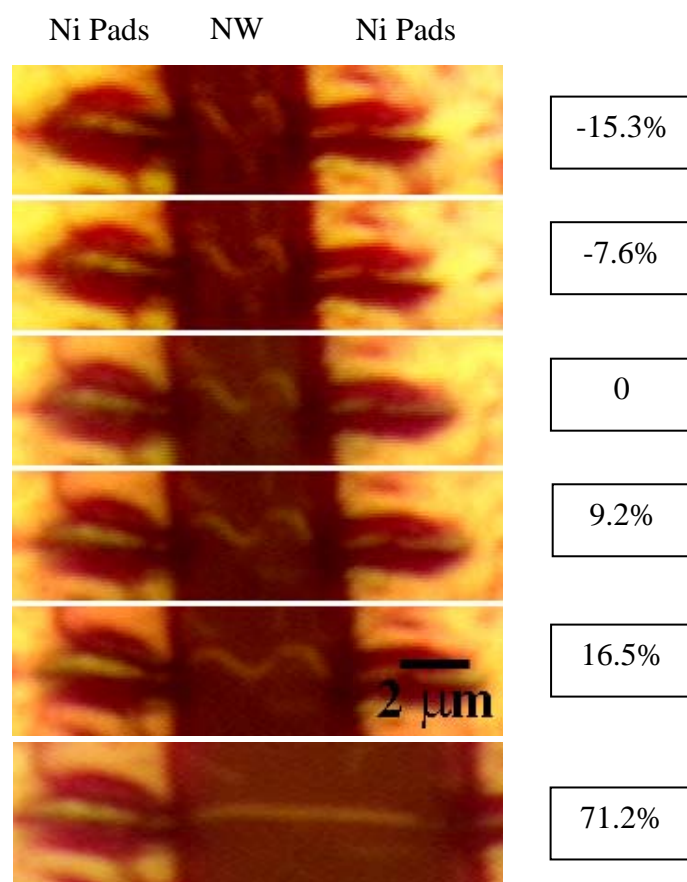


Figure S3 A sequence of optical images of the coiled NW device at different strain levels.